Fat quantification in skeletal muscle using multigradient-echo imaging: Comparison of fat and water references.

Peterson, Pernilla; Romu, Thobias; Brorson, Håkan; Dahlqvist Leinhard, Olof; Månsson, Sven

Published in:
Journal of Magnetic Resonance Imaging

DOI:
10.1002/jmri.24972

2016

Document Version:
Peer reviewed version (aka post-print)

Fat quantification in skeletal muscle using multi-gradient-echo imaging: comparison of fat and water references

Abstract

Purpose: To compare the precision, accuracy, and repeatability of water/fat imaging-based fat quantification in muscle tissue using small or large flip angles (FAs), and a water or fat reference for calculation of the proton density fat fraction (FF).

Materials and methods: An Intralipid phantom and both forearms of six patients suffering from lymphedema and ten healthy volunteers were investigated in a 1.5T scanner. Two multi-gradient-echo sequences with eight echo times and FAs of 10° and 85° were acquired, respectively. For healthy volunteers, the acquisition of the right arm was performed twice with repositioning. From each set, water reference FF and fat reference FF images were reconstructed and the average FF and the standard deviation were calculated within the subfascial compartment. The small FA water reference was considered the reference standard.

Results: The use of a fat reference effectively avoided bias due to T_1 weighting when using a large FA. The large FA fat reference approach also resulted in the highest precision, but no significant difference in repeatability between the various methods was detected.

Conclusion: The precision of fat quantification in muscle tissue can be increased with maintained accuracy using a larger flip angle, if a fat reference instead of a water reference is used.

Keywords: fat quantification, water/fat imaging, skeletal muscle, water reference, internal fat reference

Introduction

Muscular fat has been shown to be correlated to e.g. age (1), inflammation (2,3), type II diabetes mellitus (4), insulin resistance (5,6), and conditions of chronic pain (7). In this fatty depot, lipids are stored as adipocytes located between and within individual skeletal muscle groups (inter- and intramuscular fat, respectively), or as fat droplets within the muscle cells' cytoplasm (intramyocellular lipids (IMCL)). The fat concentration varies greatly over the compartment (4,8,9), and fat concentrations below 0.5 % may be expected in some muscle groups (10). Because of this, high spatial resolution imaging with accurate measurement of very low fat concentrations is an important issue for investigation of fat accumulation beneath the muscle fascia in various applications. In this method comparison study, focus is on improving precision, while maintaining accuracy of imaging-based muscular fat quantification.

Noninvasive imaging-based measurement of inter-muscular adipose tissue has previously been performed from T_1-weighted imaging where fatty and lean tissue is segmented using threshold values (5,6). Unfortunately, this technique is insensitive to the low fat concentrations expected of intramuscular fat and IMCL (8,10). This issue is partly addressed through the use of fat-selective imaging (10) which given various corrections (B_1- and B_0-inhomogeneities) and calibration against a fat reference may provide quantitative measures of fat content (8). However, a more straightforward quantification, which can be made robust against both B_0- and B_1-inhomogeneities, is possible using water/fat imaging and quantification of the proton density fat fraction (FF). Additionally, the use of quantitative images has the advantage of accounting for partial volume effects.

Water/fat imaging uses the phase evolution over echo time (TE) of gradient-echo images to separate the two signal components (11,12). The method has been extended and generalized to

account for the multipeak fat signal (13), off resonance and T_2* relaxation (14), eddy-current effects (15,16), relaxation bias (17-19), and noise (18). With consideration of these effects, high accuracy and precision of the technique has been demonstrated for liver applications (20,21). Water/fat imaging has also shown potential in vitro to accurately measure FFs below 1 % (19,22), and has recently been used for measurements of muscular fat in vivo (4,23).

The specific challenges of muscular fat quantification include demands for high signal-to-noise ratio (SNR) for measurements of low fat concentrations and consideration of relaxation bias due to the large difference in T_1 between muscle and adipose tissue (24). Both of these issues are affected by the choice of flip angle. Increased SNR is easily achieved through the use of a larger flip angle and may e.g. be adjusted to maximize the signal of the low concentration component (22). However, this approach results in an overestimation due to T_1 bias, an effect which would have been negligible if a small flip angle were used. Thus, in order to use a larger flip angle to improve SNR, an approach for correcting or avoiding T_1 bias is necessary.

The choice of reference for the estimation of the FF has an impact on T_1 bias. Commonly, a water reference is used for fat quantification; i.e. the fat signal is normalized to the sum of the fat and water signals for calculation of the FF. In this case, T_1-weighting results in an overestimation of the FF. Instead, a fat reference may be used such that the fat signal in each voxel is normalized to the signal from pure fat voxels. This approach circumvents relaxation bias in the calculation of FF, but does require selection of a fat reference tissue (external or internal) and correction for B_1-inhomogeneities (25-29).

The accuracy and precision of the water or fat reference approaches with large or small flip angles have been tested using simulations and phantom experiments (17,18,22,26,27,30), but,

to the best of our knowledge, no in vivo investigation of accuracy and precision of their use in muscular fat quantification has been presented.

The aim of this study is to conduct an in vitro and in vivo comparison of the accuracy, precision and repeatability of a small flip angle water reference approach for estimation of muscular fat against a large flip angle fat reference approach.

Material and methods

This study was approved by the local ethics committee and informed consent was obtained from all human subjects.

From multi-gradient-echo images, FF was calculated using both a water reference (wFF) and a fat reference (fFF). The calculations were made on both large and small flip angle data sets. The small flip angle wFF was used as a reference standard for all in vivo comparisons. Assuming T_1 relaxation times of muscle tissue / subcutaneous fat of 1130 ms / 288 ms at 1.5 T (24), the small flip angle was chosen such that the muscle magnetization vector had relaxed to 98 % of its full length, and the large flip angle was chosen to the Ernst angle of subcutaneous fat.

A phantom experiment was used to validate the accuracy of the techniques under investigation and to investigate the precision in regions of homogenous fat distribution. The in vivo accuracy was investigated in the entire subfascial compartment and the precision was investigated in homogenous muscle tissue of healthy volunteers and lymphedema patients. Finally, the repeatability of the technique was investigated using repeated measurements on healthy volunteers.

This methodological study was part of a clinical study aiming at investigating adipose tissue distribution in patients with lymphedema before and after liposuction.

Phantom experiment

Six Intralipid (Fresenius Kabi, Germany) phantoms were constructed in 50-mL vials and diluted with purified water to FFs 0.625 %, 1.25 %, 2.5 %, 5 %, 10 %, and 20 % (undiluted Intralipid), respectively. Also, to include a fat reference for the fFF quantification, six soybean oil phantoms were prepared in identical vials. The phantoms were placed in a water bath and imaged using a head coil with four elements in a 1.5T scanner (MAGNETOM Avanto, Siemens Healthcare, Germany). Two multi-gradient-echo sequences with eight TEs were acquired with flip angles 10° and 85°, respectively. The other sequence parameters were: TR = 600 ms, TE_1 = 1.83 ms, ΔTE = 2.47 ms, FOV = 400 x 200 mm^2, number of averages = 4, matrix = 256 x 128, and bandwidth = 1030 Hz/pixel. Three 5-mm slices were acquired and the voxel size in the reconstructed images was 5 x 1.6 x 1.6 mm^3.

Imaging of human subjects

Six patients with arm lymphedema, who had been treated with liposuction of their edematous arm one month prior to the MR examination, and ten healthy volunteers participated in this study. All imaging experiments on human subjects were conducted on a 1.5T scanner (MAGNETOM Sonata, Siemens Healthcare, Germany). For all subjects, both arms were investigated separately in a small extremity flex coil with one coil element. Note that no external fat reference was used.

To investigate the repeatability in healthy volunteers, the right arm was imaged first, followed by the left and finally, the right arm was imaged again, with repositioning of the coil between each change. All healthy subjects were placed prone with the arm to be investigated over their

head. The lymphedema patients were asked to lie prone or supine with the arm to be imaged over their head whenever possible, or otherwise to lie supine with both arms along their sides.

To compare accuracy and noise performance of two T_1-weightings, two multi-gradient-echo sequences with eight TEs were acquired with flip angles 10° and 85°, respectively. Other imaging parameters were: TR = 600 ms, TE_1 = 1.83 ms, ΔTE = 2.47 ms, FOV = 400 x 200 mm^2, number of averages = 4, matrix = 256 x 128, bandwidth = 815 Hz/pixel, and acquisition time 5 minutes and 6 seconds. Three 5-mm slices with 5-mm interslice gap were centered 10 cm distally of the humeral epicondyle and the voxel size of the reconstructed images was 5 x 1.6 x 1.6 mm^3.

Reconstructions

An iterative least-squares algorithm combining magnitude (for the first echo) and complex (remaining echoes) data was used for separation of complex fat and water signals from the small and large flip-angle data sets (15). The off-line algorithm was implemented in Matlab (R2013a, Mathworks, USA). The combined fitting procedure was chosen to avoid eddy-current effects of the first echo acquired. The signal model included a precalibrated multipeak fat model with eight fat resonances (13,31), off resonance and T_2* dephasing (14). The relative amplitudes of the eight fat peaks were estimated based on the theoretical expressions suggested by Hamilton et al (31) assuming 2.89 double bonds per triglyceride in adipose tissue (31,32). A single T_2* was chosen because of the superior noise performance at low fat concentrations compared to dual T_2* estimation (33,34). A first guess for off resonance was used to avoid fat/water ambiguity and was obtained using the procedure described in (35) for in vivo data, and using the phase differences between adjacent echoes for phantom data.

The reconstructions resulted in two sets of complex-valued fat (F) and water (W) images for each of the phantom and in vivo experiments: **1)** small flip angle and **2)** large flip angle. From each of these data sets, **A)** wFF and **B)** fFF were calculated.

The wFF was calculated using the following expression where the real value was used to avoid bias due to the Rician noise distribution of magnitude images (36):

$$wFF = \mathrm{Re}\left(\frac{F}{F+W}\right) \qquad [1]$$

The estimation of fFF images uses pure adipose tissue voxels as an internal fat reference and is illustrated in Figure 1. The fFF was calculated from the same set of separated F and W images (Figure 1a,b) as used for the estimation of wFF (Figure 1c). Signal intensity variations due to B_1 and coil sensitivity inhomogeneity were estimated by observing that the fat intensity of pure adipose tissue voxels (Figure 1d) should be spatially independent. Thus, a fat intensity bias field B_{fat} (Figure 1e) could be calculated by locating adipose tissue voxels (identified as non-background voxels with wFF > 95 %) and interpolating the intensities of these to the remaining voxels of B_{fat}. The intensity corrected fFF image was then calculated as fFF = F/B_{fat} (Figure 1f).

The fFF image is thus obtained by normalizing the local intensity of F with the average intensity of nearby adipose tissue voxels. This is a non-trivial operation since the uncertainty of the estimate increases with the distance from the references, and no assumptions can be made regarding the spatial distribution of the reference voxels. B_{fat} was calculated by multi scale adaptive normalized averaging (MANA), as described briefly below (see reference (29) for further details). This algorithm interpolates/extrapolates the intensity values of the reference

voxels to all non-reference voxels by local weighted averaging. The weights are set by Gaussian kernels which variance increase as the local density decrease. Thus voxel estimates in low density areas will be based on a larger spatial support. In addition, since the MANA algorithm uses real-valued images, the *F* and *W* images were phase unwrapped as real-valued images. The phase unwrapping was performed on the *F+W* image using phase sensitive reconstruction (37). The unwrapped phase was subtracted from the *F* and *W* images, respectively.

Evaluation

Circular regions-of-interest (ROIs) were drawn in each phantom vial in the magnitude image of the first echo acquired. In the corresponding in vivo images, polygonal ROIs were manually drawn covering the subfascial compartment, excluding bone and bone marrow. Close to bone and the muscle fascia, a margin of approximately one pixel was avoided. Also, circular ROIs were drawn in homogenous muscle tissue using the large flip angle wFF images. All ROIs were copied and identical for the two flip angles and the water and fat reference data sets. Within all ROIs, the FF average and standard deviation were calculated.

Accuracy

Using the small flip angle wFF as a reference standard, the accuracy of muscular FF quantification was investigated for small and large flip angles, for both water and fat referenced FFs. The slope, intercept, overall bias and limits of agreement were used as measures of accuracy. A Wilcoxon signed rank test with $P < 0.05$ was used to test overall biases for significant difference from a zero bias.

Precision

The FF standard deviation within homogenous muscle tissue was used as a measure of precision. A two-sided t-test was used to test for differences between the precisions of the various methods. A significance level of $P < 0.05$ was used.

Repeatability

The repeatabilities of the two muscular FF quantification approaches were investigated using the repeated measurement of the right forearm of healthy subjects. The measured FF was compared between the two measurements, and an overall bias and coefficient of repeatability (1.96 times the standard deviation of differences between measurements) were calculated. For the various methods, the absolute values of the differences between the two repetitions were compared using a Wilcoxon signed rank test with $P < 0.05$.

Results

Phantom experiment

The resulting phantom small and large flip angle FF maps are shown in Figure 2 and the numerical results are presented in Figure 3. Accurate quantification of the FF was achieved using a fat reference with both small and large flip angles. As expected, the use of a large flip angle for estimation of wFF resulted in an overestimation of the FF, whereas high agreement with known values was obtained using a small flip angle.

Comparing the standard deviations within ROIs for all methods (Figure 3, lower row), the precision was highest (smallest standard deviation) using fFF and a large flip angle. Out of all methods, the poorest precision was obtained using fFF with a small flip angle. As expected, a higher precision was obtained through the use of a large flip angle compared to a small flip angle for wFF estimation, especially for FF $\leq$ 2.5 %. The observed difference was smaller for higher FFs. Some signal variation may be attributed to Gibbs ringing which was visible in the reconstructed phantom images.

In vivo experiment

Examples of small flip angle wFF and large flip angle fFF maps from healthy volunteers and one lymphedema patient are shown in Figure 4 and 5, respectively. The estimation of fFF failed

in one of the ten healthy volunteer cases (Figure 4c), likely because of the thin layer of subcutaneous adipose tissue. Due to the limited resolution and partial-volume effects, the fat reference tissue was not sufficient for reconstruction. This subject was therefore excluded from further analysis.

The median (range) subfascial FF in percent over three 5-mm slices for the right/left/right arm of healthy volunteers was 2.1 (1.7-5.2) / 1.2 (0.5-5.0) / 2.1 (1.7-4.9). The corresponding values for the edematous/control arm in patients were 7.2 (3.0-8.5) / 5.1 (3.5-7.0).

Accuracy

The accuracy of the muscular large flip angle fFFs compared to reference is shown as scatter and Bland-Altman plots in Figure 6. The accuracy measures for all tested methods as compared to reference are provided in Table 1. The use of a large flip angle in combination with a fat reference estimation of the FF effectively avoids T_1 bias and results in an accurate result compared to the small flip angle wFF. Using a large flip angle fFF, the overall bias was calculated to 0.31 % as compared to 1.74 % using a large flip angle wFF.

Precision

The FF standard deviations within a circular ROI placed in homogenous muscle tissue are compared between the small flip angle wFF and the large flip angle fFF methods in Figure 7. The average standard deviation of all subjects were 2.1 % for the small flip angle wFF, 1.7 % for the large flip angle wFF, 2.1 % for the small flip angle fFF, and 1.3 % for the large flip angle fFF. The precision of the large flip angle fFF was significantly higher than all other tested methods. The differences in precision between all tested methods were significant, expect between the small flip angle fat and water reference FFs.

Repeatability

The results from the repeatability experiment using the small flip angle wFF and large flip angle fFF methods are shown as Bland-Altman plots in Figure 8, and corresponding biases and coefficients of repeatability for all tested approaches are presented in Table 2. The coefficients of repeatability using a small flip angle were similar for both the fFF and wFF, whereas the coefficients of repeatability were slightly larger using a large flip angle with both references. The coefficient of repeatability of the large flip angle fFF was slightly smaller than the corresponding wFF. No significant differences in coefficients of repeatability were found between any of the methods tested.

Discussion

In this study, the accuracy, precision, and repeatability of muscular fat quantification based on FF and MRI was investigated. In addition, two references for FF quantification and two flip angle approaches were compared. Due to the low FFs expected in muscle tissue, and due to the large differences in longitudinal relaxation times between adipose and muscle tissues, FF quantification beneath the muscle fascia calls for careful consideration of both SNR and relaxation bias. In this study, we investigated if the use of a large flip angle in combination with the use of a fat reference to circumvent quantification bias due to T_1 weighting could improve FF quantification. A high agreement with the reference standard and an improved precision was seen for the large flip angle method with a fat reference. In terms of repeatability, no significant difference between the methods was detected.

Using a small flip angle and a water reference, differences in muscular FF larger than approximately 0.4 % can be detected according to our repeatability investigation (see Table 2). Relating to our own measurements, where average FFs ranged between 0.5 % – 5.2 % for healthy volunteers and between 3.0 % – 8.5 % for patients, a coefficient of repeatability of

approximately 0.4 % is sufficient to resolve the differences between patients within each of these groups. The accuracy of the fat reference approach with large flip angle was similar to the reference standard, and measurements were within approximately ± 1.8 % (see Table 1). Also, the precision within homogenous muscle tissue was improved using this technique. This gain in precision might be useful e.g. for quantification of intramuscular adipose tissue and IMCL.

A small flip angle approach is commonly used to avoid T_1 bias. However, this approach limits the SNR achievable in a reasonable imaging time. Instead, a larger flip angle may be used if T_1 bias is avoided or corrected for. In this work, the use of a fat reference for FF quantification was explored. Alternatively, T_1 bias may be corrected for using literature values of the T_1 relaxation time of the fat and water signals (38) or using a dual flip angle approach which simultaneously estimates a corrected FF and the fat and water T_1 values (18,30). Depending on method chosen, the optimal flip angle or pair of flip angles may differ. In this study, no attempt was made to explore the optimal choice of flip angle/s, nor was the dual flip angle approach investigated.

In this study, the MANA algorithm was used for estimation of fFF, which uses an internal fat reference and does not require additional data to be acquired (29). This allows for effective data acquisition and calibration to the subject's own adipose tissue. The MANA algorithm has previously been successfully used for reconstruction of whole-body, 3D data sets (29), for intensity correction of muscle and liver water imaging (25) and for identification of brown adipose tissue (39).

The use of a fat reference for FF quantification has distinctive advantages and disadvantages. First, our phantom and in vivo results show that the use of a fat reference effectively

circumvents T_1-relaxation-related bias and that a similarly high accuracy is obtained with a large flip angle fFF compared to a small flip angle wFF. The large flip angle fFF approach also improved precision compared to small flip angle wFF. As the method is insensitive to T_1-related bias, it allows for a more flexible choice of imaging parameters. E.g. the flip angle may be increased to improve SNR, as was done in this study, or the TR may be shortened for more efficient data acquisition and a shorter acquisition time. Second, the fFF measure is insensitive to cases where the assumption that MR-visible water and/or fat constitutes the entire voxel volume may not hold. Third, the presence of adipose tissue is necessary for successful reconstruction of fFF images. In this study, all cases but one resulted in successful fFF reconstruction. The patient dataset was challenging as the patient subjects had undergone liposuction one month prior to the MRI examination, but the successful reconstructions of all images from the patient group indicate that the remaining adipose tissue was sufficient as a fat reference. However, in one healthy control, the image resolution was not sufficient to resolve the subcutaneous fat layer. Thus, for the use of a fat reference, consideration of image resolution is important. In addition, the threshold used to identify pure fat reference voxels may have an impact on the success of the method in these cases (see below). As opposed to the three 2D slices used in this work, the robustness of the MANA algorithm is likely improved using a 3D acquisition over a larger volume as more adipose tissue may be used as reference (25).

The threshold for pure fat voxels was in this study set to voxels with wFF > 95 %. Lowering this threshold would result in a larger number of voxels to use as reference in the MANA algorithm which might be an advantage in cases of very thin subcutaneous layers. However, a lowered threshold may also result in an overestimation of the fFF.

Within a homogenous area of muscle tissue, no difference in precision was found between the small flip angle fat and water reference FFs. This implies that the precision of the water and fat reference estimation methods are similar if there is no T_1 weighting. Compared to a low flip angle approach, the FF precision was found to be higher for a large flip angle fFF approach, but very little improvement in precision was seen for a large flip angle wFF approach. This is likely explained by T_1 weighting of fatty streaks in muscle tissue leading to an enhancement of anatomical variance when using a larger flip angle and a water reference approach. This apparent increase of the anatomical variance overshadows the reduction of image noise when comparing small and large flip angle wFF standard deviations. The use of standard deviation within ROIs as a measure of precision is limited by the inability to distinguish between measurement precision and anatomical variance. However, the in vivo measurements were complemented by measurements in homogenous lipid phantoms to account for this issue. Also in this experiment, a gain in precision using a large flip angle and fat reference was seen compared to the other techniques investigated. Despite the gain in precision found using a large flip angle fFF, no improvement of repeatability was seen for this technique compared to reference.

In conclusion, a fat reference for FF quantification can be used to improve precision and avoid T_1 bias in muscle fat quantification. However, for robust estimation of fat reference FF, image resolution must be considered. In cases where very little adipose tissue is expected, a small flip angle wFF approach may be more reliable.

Acknowledgements

The authors are grateful for helpful discussions with Lars E. Olsson, Lund University and H. Harry Hu, Phoenix Children's Hospital.

References

1. Delmonico MJ, Harris TB, Visser M, Park SW, Conroy MB, Velasquez-Mieyer P, Boudreau R, Manini TM, Nevitt M, Newman AB, Goodpaster BH. Longitudinal study of muscle strength, quality, and adipose tissue infiltration. Am J Clin Nutr 2009;90(6):1579-1585.
2. Beasley LE, Koster A, Newman AB, Javaid MK, Ferrucci L, Kritchevsky SB, Kuller LH, Pahor M, Schaap LA, Visser M, Rubin SM, Goodpaster BH, Harris TB. Inflammation and race and gender differences in computerized tomography-measured adipose depots. Obesity (Silver Spring) 2009;17(5):1062-1069.
3. Zoico E, Rossi A, Di Francesco V, Sepe A, Olioso D, Pizzini F, Fantin F, Bosello O, Cominacini L, Harris TB, Zamboni M. Adipose tissue infiltration in skeletal muscle of healthy elderly men: relationships with body composition, insulin resistance, and inflammation at the systemic and tissue level. J Gerontol A Biol Sci Med Sci 2010;65(3):295-299.
4. Karampinos DC, Baum T, Nardo L, Alizai H, Yu H, Carballido-Gamio J, Yap SP, Shimakawa A, Link TM, Majumdar S. Characterization of the regional distribution of skeletal muscle adipose tissue in type 2 diabetes using chemical shift-based water/fat separation. J Magn Reson Imaging 2012;35(4):899-907.
5. Boettcher M, Machann J, Stefan N, Thamer C, Haring HU, Claussen CD, Fritsche A, Schick F. Intermuscular adipose tissue (IMAT): association with other adipose tissue compartments and insulin sensitivity. J Magn Reson Imaging 2009;29(6):1340-1345.
6. Gallagher D, Kuznia P, Heshka S, Albu J, Heymsfield SB, Goodpaster B, Visser M, Harris TB. Adipose tissue in muscle: a novel depot similar in size to visceral adipose tissue. Am J Clin Nutr 2005;81(4):903-910.
7. Elliott J, Pedler A, Kenardy J, Galloway G, Jull G, Sterling M. The temporal development of fatty infiltrates in the neck muscles following whiplash injury: an association with pain and posttraumatic stress. PLoS One 2011;6(6):e21194.
8. Goodpaster BH, Stenger VA, Boada F, McKolanis T, Davis D, Ross R, Kelley DE. Skeletal muscle lipid concentration quantified by magnetic resonance imaging. Am J Clin Nutr 2004;79(5):748-754.
9. Machann J, Bachmann OP, Brechtel K, Dahl DB, Wietek B, Klumpp B, Haring HU, Claussen CD, Jacob S, Schick F. Lipid content in the musculature of the lower leg assessed by fat selective MRI: intra- and interindividual differences and correlation with anthropometric and metabolic data. J Magn Reson Imaging 2003;17(3):350-357.
10. Schick F, Machann J, Brechtel K, Strempfer A, Klumpp B, Stein DT, Jacob S. MRI of muscular fat. Magn Reson Med 2002;47(4):720-727.
11. Dixon WT. Simple proton spectroscopic imaging. Radiology 1984;153(1):189-194.
12. Reeder SB, Wen Z, Yu H, Pineda AR, Gold GE, Markl M, Pelc NJ. Multicoil Dixon chemical species separation with an iterative least-squares estimation method. Magn Reson Med 2004;51(1):35-45.
13. Yu H, Shimakawa A, McKenzie CA, Brodsky E, Brittain JH, Reeder SB. Multiecho water-fat separation and simultaneous R2* estimation with multifrequency fat spectrum modeling. Magn Reson Med 2008;60(5):1122-1134.
14. Yu H, McKenzie CA, Shimakawa A, Vu AT, Brau AC, Beatty PJ, Pineda AR, Brittain JH, Reeder SB. Multiecho reconstruction for simultaneous water-fat decomposition and T2* estimation. J Magn Reson Imaging 2007;26(4):1153-1161.
15. Hernando D, Hines CD, Yu H, Reeder SB. Addressing phase errors in fat-water imaging using a mixed magnitude/complex fitting method. Magn Reson Med 2012;67(3):638-644.

16. Yu H, Shimakawa A, Hines CD, McKenzie CA, Hamilton G, Sirlin CB, Brittain JH, Reeder SB. Combination of complex-based and magnitude-based multiecho water-fat separation for accurate quantification of fat-fraction. Magn Reson Med 2011;66(1):199-206.
17. Bydder M, Yokoo T, Hamilton G, Middleton MS, Chavez AD, Schwimmer JB, Lavine JE, Sirlin CB. Relaxation effects in the quantification of fat using gradient echo imaging. Magn Reson Imaging 2008;26(3):347-359.
18. Liu CY, McKenzie CA, Yu H, Brittain JH, Reeder SB. Fat quantification with IDEAL gradient echo imaging: correction of bias from T(1) and noise. Magn Reson Med 2007;58(2):354-364.
19. Mansson S, Peterson P, Johansson E. Quantification of low fat contents: a comparison of MR imaging and spectroscopy methods at 1.5 and 3 T. Magn Reson Imaging 2012;30(10):1461-1467.
20. Hines CD, Frydrychowicz A, Hamilton G, Tudorascu DL, Vigen KK, Yu H, McKenzie CA, Sirlin CB, Brittain JH, Reeder SB. T(1) independent, T(2) (*) corrected chemical shift based fat-water separation with multi-peak fat spectral modeling is an accurate and precise measure of hepatic steatosis. J Magn Reson Imaging 2011;33(4):873-881.
21. Meisamy S, Hines CD, Hamilton G, Sirlin CB, McKenzie CA, Yu H, Brittain JH, Reeder SB. Quantification of Hepatic Steatosis with T1-independent, T2*-corrected MR Imaging with Spectral Modeling of Fat: Blinded Comparison with MR Spectroscopy. Radiology 2011;258(3):767-775.
22. Ballweg V, Wojtczyk H, Roth N, Martirosian P, Springer F, Schick F. Optimized in-phase and opposed-phase MR imaging for accurate detection of small fat or water fractions: theoretical considerations and experimental application in emulsions. MAGMA 2011;24(3):167-178.
23. Kovanlikaya A, Mittelman SD, Ward A, Geffner ME, Dorey F, Gilsanz V. Obesity and fat quantification in lean tissues using three-point Dixon MR imaging. Pediatr Radiol 2005;35(6):601-607.
24. Gold GE, Han E, Stainsby J, Wright G, Brittain J, Beaulieu C. Musculoskeletal MRI at 3.0 T: relaxation times and image contrast. AJR American journal of roentgenology 2004;183(2):343-351.
25. Andersson T, Romu T, Karlsson A, Noren B, Forsgren MF, Smedby O, Kechagias S, Almer S, Lundberg P, Borga M, Leinhard OD. Consistent intensity inhomogeneity correction in water-fat MRI. J Magn Reson Imaging 2014.
26. Cui Y, Yang IY, Wade T, Wiens CN, Soliman AS, McKenzie CA. Absolute Quantification of In Vio Water and Fat Content. In: Proceedings of the 20th Annual Meeting of ISMRM. Melbourne, Australia2012. p 363.
27. Hu HH, Nayak KS. Quantification of absolute fat mass using an adipose tissue reference signal model. J Magn Reson Imaging 2008;28(6):1483-1491.
28. Leinhard OD, Johansson A, Rydell J, Smedby O, Nystrom F, Lundberg P, Borga M. Quantitative abdominal fat estimation using MRI. 19th International Conference on Pattern Recognition, Vols 1-6 2008:2137-2140.
29. Romu T, Borga M, Leinhard OD. Mana - Multi Scale Adaptive Normalized Averaging. 2011 8th Ieee International Symposium on Biomedical Imaging: From Nano to Macro 2011:361-364.
30. Karampinos DC, Yu H, Shimakawa A, Link TM, Majumdar S. T(1)-corrected fat quantification using chemical shift-based water/fat separation: application to skeletal muscle. Magn Reson Med 2011;66(5):1312-1326.

31. Hamilton G, Yokoo T, Bydder M, Cruite I, Schroeder ME, Sirlin CB, Middleton MS. In vivo characterization of the liver fat (1)H MR spectrum. NMR in biomedicine 2011;24(7):784-790.
32. Ren J, Dimitrov I, Sherry AD, Malloy CR. Composition of adipose tissue and marrow fat in humans by 1H NMR at 7 Tesla. Journal of lipid research 2008;49(9):2055-2062.
33. Chebrolu VV, Hines CD, Yu H, Pineda AR, Shimakawa A, McKenzie CA, Samsonov A, Brittain JH, Reeder SB. Independent estimation of T*2 for water and fat for improved accuracy of fat quantification. Magnetic resonance in medicine : official journal of the Society of Magnetic Resonance in Medicine / Society of Magnetic Resonance in Medicine 2010;63(4):849-857.
34. Hernando D, Liang ZP, Kellman P. Chemical shift-based water/fat separation: a comparison of signal models. Magn Reson Med 2010;64(3):811-822.
35. Berglund J, Johansson L, Ahlstrom H, Kullberg J. Three-point Dixon method enables whole-body water and fat imaging of obese subjects. Magn Reson Med 2010;63(6):1659-1668.
36. Gudbjartsson H, Patz S. The Rician distribution of noisy MRI data. Magn Reson Med 1995;34(6):910-914.
37. Rydell J, Knutsson H, Pettersson J, Johansson A, Farneback G, Dahlqvist O, Lundberg P, Nystrom F, Borga M. Phase sensitive reconstruction for water/fat separation in MR imaging using inverse gradient. Med Image Comput Comput Assist Interv 2007;10(Pt 1):210-218.
38. Yang IY, Cui Y, Wiens CN, Wade TP, Friesen-Waldner LJ, McKenzie CA. Fat fraction bias correction using T estimates and flip angle mapping. J Magn Reson Imaging 2013. doi: 10.1002/jmri.24126.
39. Lidell ME, Betz MJ, Dahlqvist Leinhard O, Heglind M, Elander L, Slawik M, Mussack T, Nilsson D, Romu T, Nuutila P, Virtanen KA, Beuschlein F, Persson A, Borga M, Enerback S. Evidence for two types of brown adipose tissue in humans. Nat Med 2013;19(5):631-634.

Tables

Table 1. Measures of FF quantification accuracy for fat and water references with small and large flip angles compared to a small flip angle water reference fat fraction.

	Small flip angle	**Large flip angle**
Water reference		
Slope	-	1.39 ± 0.18
Intercept (%)	-	0.38 ± 0.73
Bias (%)	-	1.74
Limits of agreement (%)	-	[-1.03; 4.50]
Fat reference		
Slope	0.86 ± 0.09	0.94 ± 0.15
Intercept (%)	0.09 ± 0.39	0.19 ± 0.27
Bias (%)	-0.38*	0.31
Limits of agreement (%)	[-1.67; 0.90]	[-1.51; 2.14]

* Significantly different from zero with $P < 0.05$

Table 2. Measures of repeatability of FF estimation with water and fat references with small and large flip angle data.

	Small flip angle	**Large flip angle**
Water reference		
Bias (%)	-0.05	-0.05
Coefficient of repeatability (%)	0.41	0.82
Fat reference		
Bias (%)	-0.20	0.06
Coefficient of repeatability (%)	0.54	0.62

Figure captions

Figure 1. Illustration of the fFF calculation. The method uses *F* (a) and *W* (b) as input. From these, the wFF is calculated (c). An internal fat reference is chosen as wFF > 95 % (d). Using *F* and the fat reference, MANA calculates a fat intensity bias field B_{fat} (e). Finally, fFF is calculated by dividing *F* with B_{fat} (f). The improvement compared to *F* can be seen in the histogram (g).

Figure 2. Phantom small (left) and large (right) flip angle wFF (top) and fFF (bottom) maps. The color scale represents a FF range from 0 % (blue) to 100 % (red). Six soybean oil vials (three in top and three on bottom) were included to provide a fat reference for fFF reconstruction. The two center rows of vials contain Intralipid/water mixtures with FFs ranging from 20 % (top left) to 0.63 % (bottom right). The large flip angle wFFs are higher compared to the large flip angle fFFs.

Figure 3. Results of accuracy (top row) and precision (bottom row) analysis of Intralipid phantom data using estimation of wFF (left column) and fFF (right column). In the top row diagrams, the mean within ROIs in six Intralipid phantom vials are plotted against the known fat concentrations. In the bottom row diagrams, standard deviations within ROIs are plotted against known fat concentrations. The FF overestimation using a large flip angle wFF is avoided using large flip angle fFF. The lowest standard deviations are seen for large flip angle fFFs.

Figure 4. Examples of small flip angle wFF (top row) and large flip angle fFF (bottom row) maps of the right arm of three healthy volunteers. The color scale represents a FF range from 0 % (blue) to 100 % (red). Examples a and b show successful reconstructions of both wFF and fFF, whereas the subcutaneous adipose layer was too thin for a successful fFF reconstruction

in Example c (small flip angle fFF shown to highlight artefacts). This subject was excluded from further analysis.

Figure 5. Examples of small flip angle wFF (top row) and large flip angle fFF (bottom row) maps of the edematous, liposuctioned arm (left column) and healthy arm (right column) of a lymphedema patient. The color scale represents a FF range from 0 % (blue) to 100 % (red). Only small areas of adipose tissue remain in the subcutaneous layer of the liposuctioned arm.

Figure 6. Accuracy of average FF estimates in healthy subjects and patients. The top figure show a scatter plot and the bottom a Bland-Altman plot of large flip angle fFF as compared to small flip angle wFF. In the scatter plot, the line of identity is shown in solid black and a linear regression is shown as a dashed black line. In the Bland-Altman plot, the average bias is shown in solid black and limits of agreement are visualized as dashed black lines. T_1 bias is effectively avoided using a large flip angle fFF.

Figure 7. Precision analysis comparing small flip angle wFF (blue) and large flip angle fFF (red) in healthy subjects and patients. A lower average standard deviation (solid line) is seen for the large flip angle fFF.

Figure 8. Bland-Altman small flip angle wFF (left) and large flip angle fFF (right) repeatability analysis in healthy subjects. The smallest coefficient of repeatability is seen for small flip angle wFF, and the largest for large flip angle fFF.

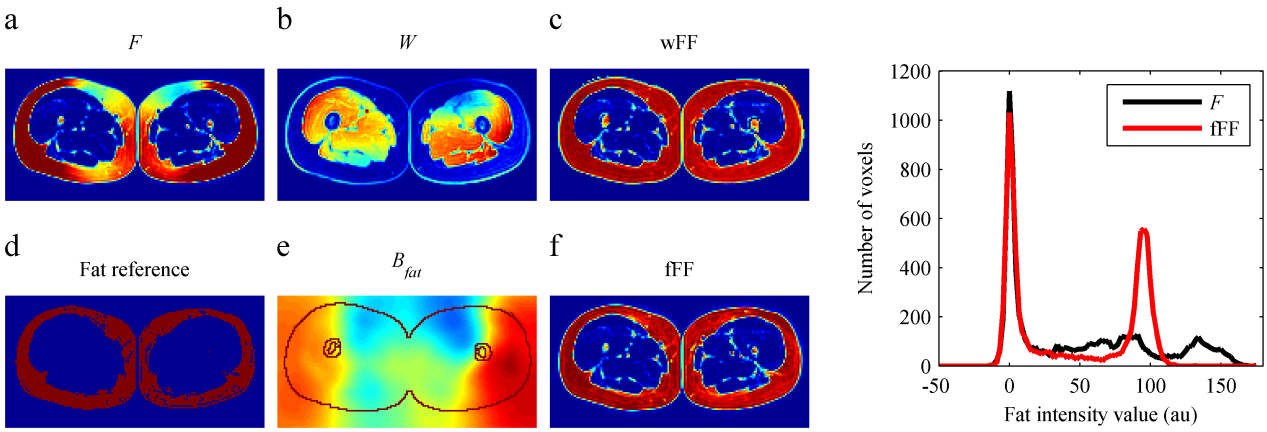
a
F
b
W
c
wFF
d
Fat reference
e
B_{fat}
f
fFF
1200
1000
800
600
400
200
0
-50
0
50
100
150
Number of voxels
Fat intensity value (au)
F
fFF

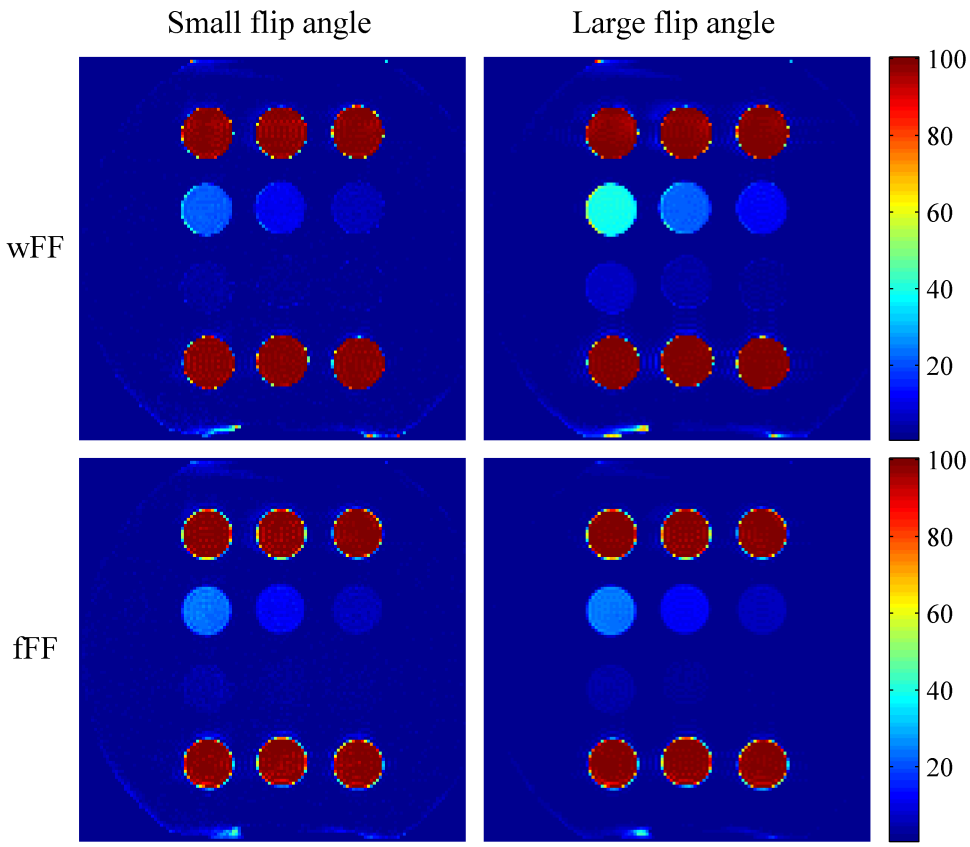
Small flip angle
Large flip angle
wFF
fFF
100
80
60
40
20
100
80
60
40
20

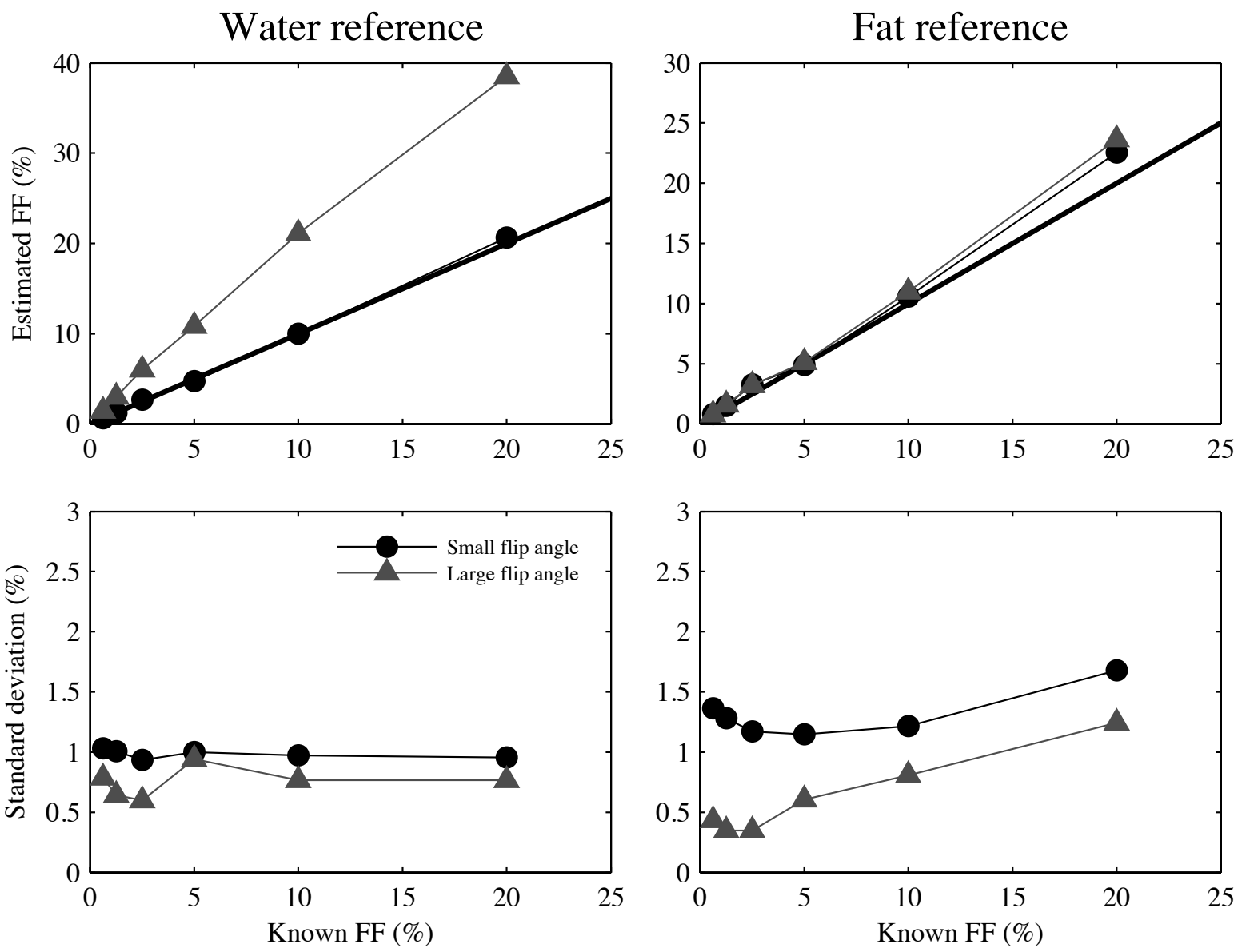
Water reference
Fat reference
Estimated FF (%)
Standard deviation (%)
Known FF (%)
Known FF (%)
Small flip angle
Large flip angle

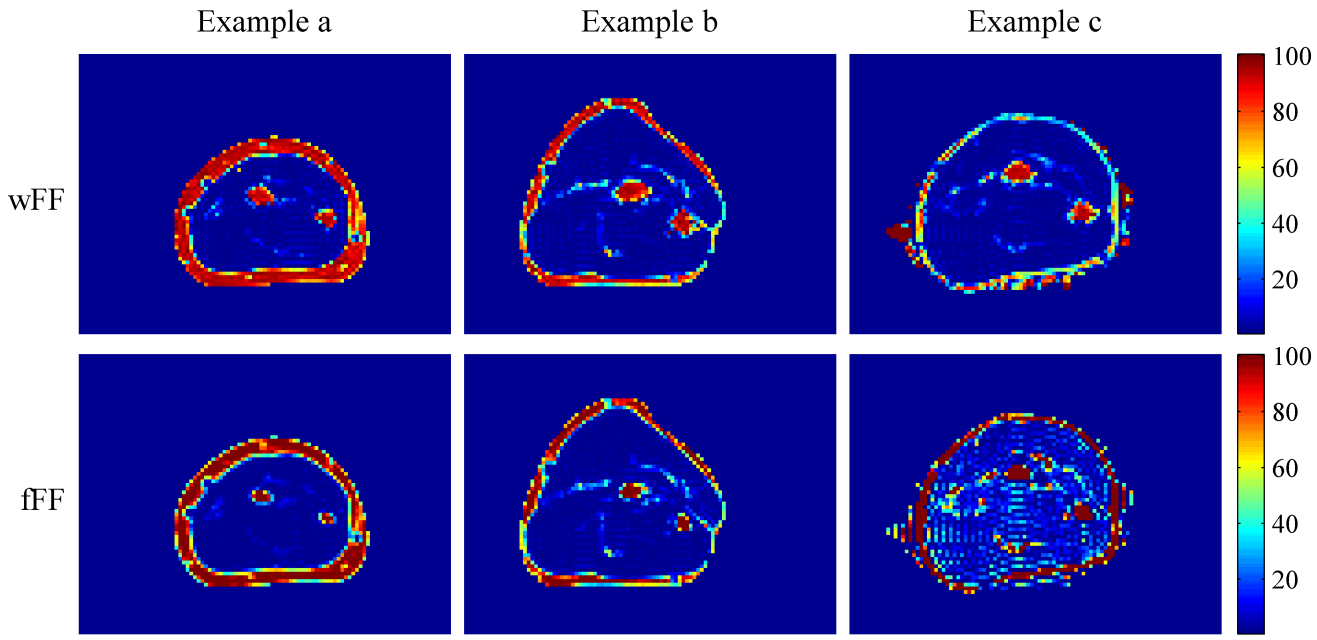
Example a
Example b
Example c
wFF
fFF
100
80
60
40
20
100
80
60
40
20

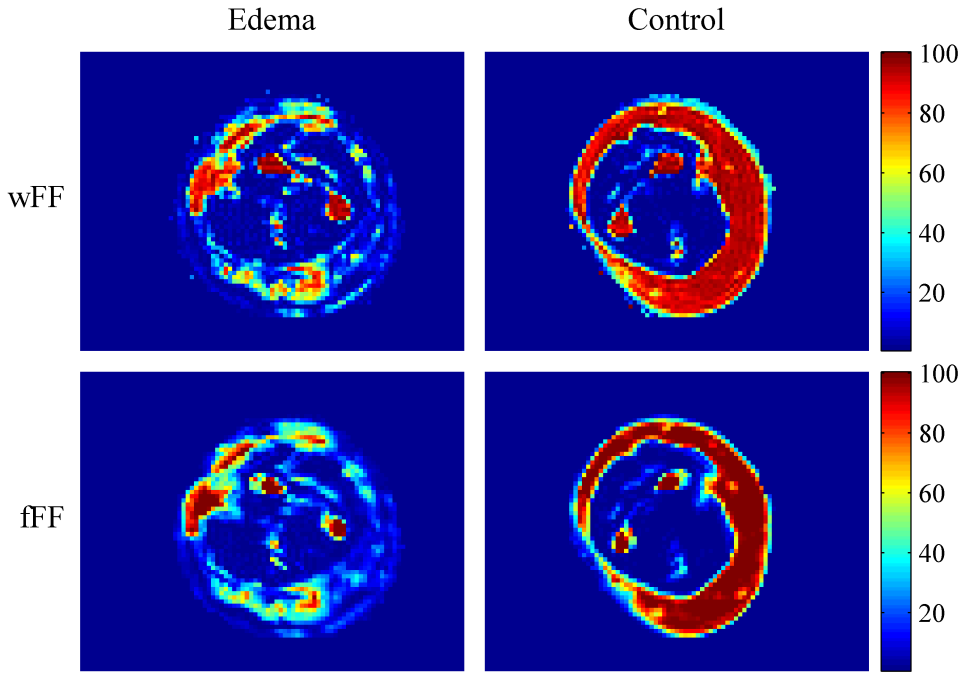
Edema
Control
wFF
fFF
100
80
60
40
20
100
80
60
40
20

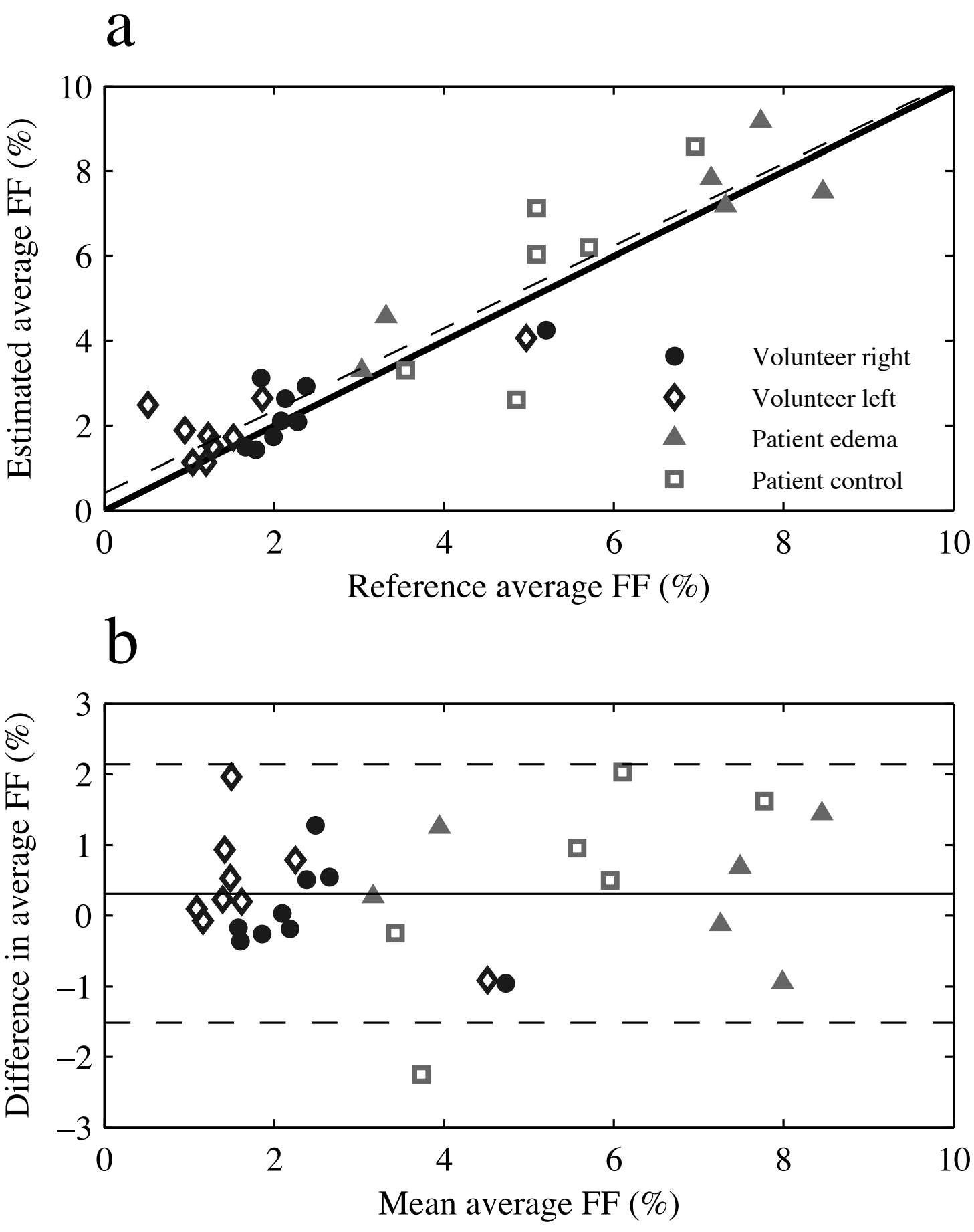
a
Estimated average FF (%)
Reference average FF (%)
Volunteer right
Volunteer left
Patient edema
Patient control
b
Difference in average FF (%)
Mean average FF (%)

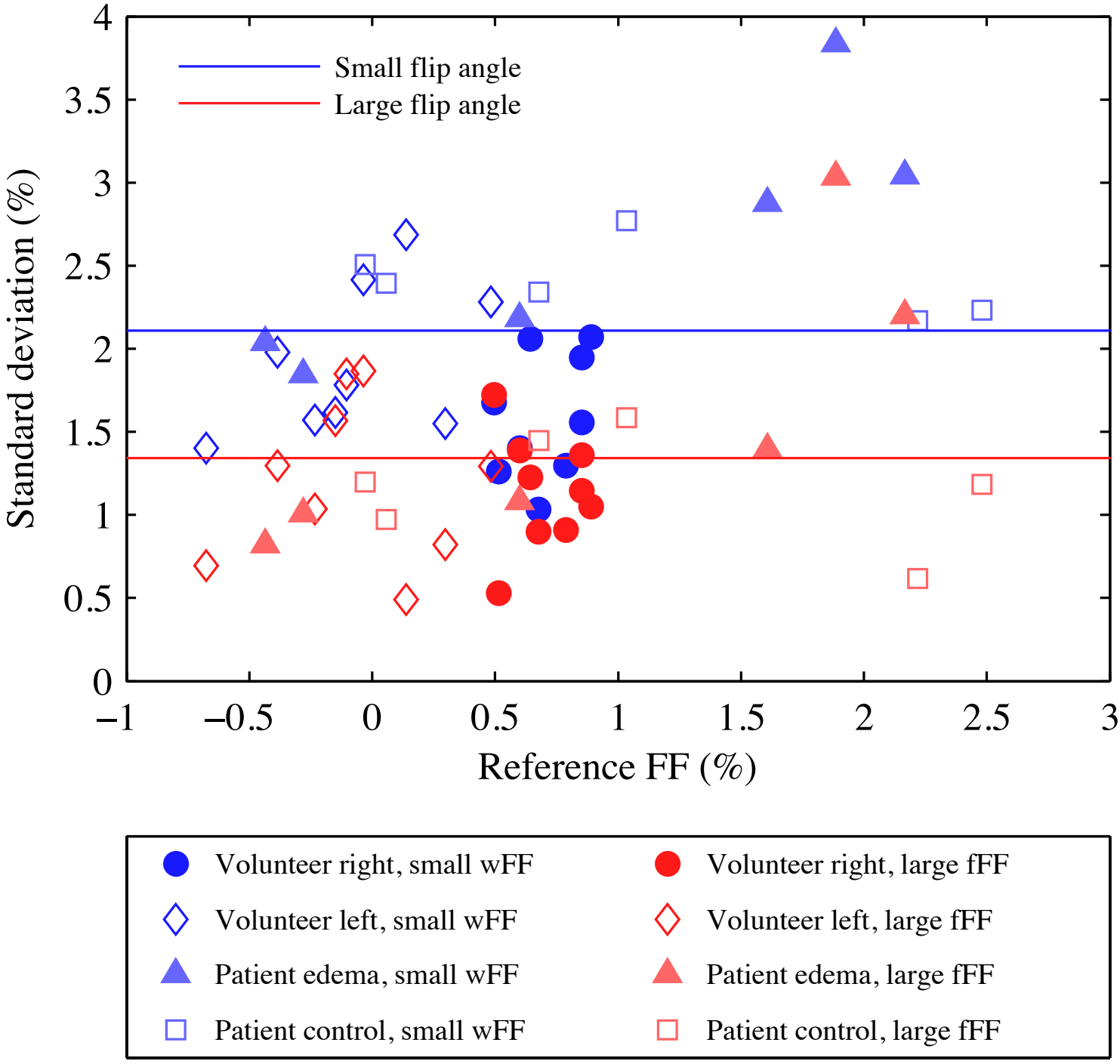
Small flip angle
Large flip angle
Standard deviation (%)
Reference FF (%)
4
3.5
3
2.5
2
1.5
1
0.5
0
−1
−0.5
0
0.5
1
1.5
2
2.5
3
Volunteer right, small wFF
Volunteer right, large fFF
Volunteer left, small wFF
Volunteer left, large fFF
Patient edema, small wFF
Patient edema, large fFF
Patient control, small wFF
Patient control, large fFF

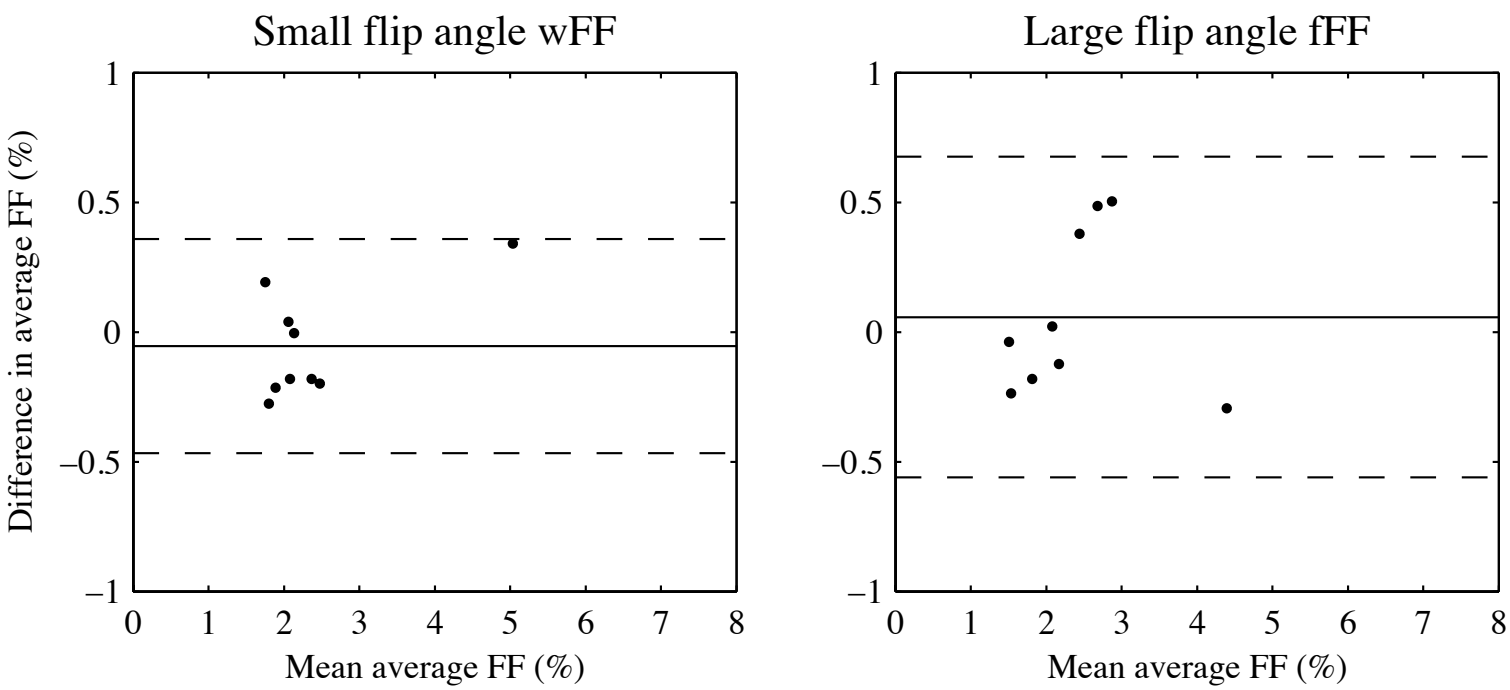
Small flip angle wFF
Large flip angle fFF
Difference in average FF (%)
Mean average FF (%)
Mean average FF (%)
1
0.5
0
−0.5
−1
0
1
2
3
4
5
6
7
8